Tellus (2007), 59, 654–663
Printed in Singapore. All rights reserved

TELLUS

Temporal variations of atmospheric carbon dioxide in the southernmost part of Japan

By XIA ZHANG[1]*, TAKAKIYO NAKAZAWA[1], MISA ISHIZAWA[2], SHUJI AOKI[1], SHIN-ICHIRO NAKAOKA[1], SATOSHI SUGAWARA[3], SHAMIL MAKSYUTOV[4], TAZU SAEKI[5] and TADAHIRO HAYASAKA[5], [1]*Center for Atmospheric and Oceanic Studies, Tohoku University, Sendai 980-8578, Japan;* [2]*Air Quality Research Division, Environment Canada, Toronto, Ontario M3H 5T4, Canada;* [3]*Miyagi University of Education, Sendai 980-0845, Japan;* [4]*National Institute for Environmental Studies, Tsukuba 305-8506, Japan;* [5]*Research Institute for Human and Nature, Kyoto 602-0878, Japan*

(Manuscript received 3 October 2006; in final form 17 April 2007)

ABSTRACT

We present analysis of the temporal variation of atmospheric CO_2 in the subtropical region of East Asia, obtained aboard a ferry between Ishigaki Island and Hateruma Island, Japan for the period June 1993–April 2005. The annual mean CO_2 concentration increases from 360.1 ppmv in 1994 to 378.4 ppmv in 2004, showing an average growth rate of 1.8 ppmv yr^{-1}. The growth rate shows interannual variations with high values during ENSO events. The average seasonal CO_2 cycle reaches the maximum in early April and the minimum in mid-September, with a peak-to-peak amplitude of 8.5 ppmv. Numerical simulations using a three-dimensional atmospheric transport model show interannual variations of the CO_2 growth rate similar to the observation, but the amplitude of the seasonal cycle is larger, with maximum concentration appearing earlier than the observation by 1 month. Low CO_2 values observed during the spring of 1998 are likely associated with the 1997/1998 ENSO event. A backward trajectory analysis suggests that they were due to changes in atmospheric transport whereby maritime air masses from the Pacific Ocean dominated over polluted air masses from the Asian Continent. Extreme values (either high or low) of CO_2 are also occasionally observed. A comparison of backward trajectories of air parcels with CO_2 concentration fields calculated using the atmospheric transport model shows that these unusual CO_2 concentrations result from the transport of air affected not only by anthropogenic CO_2 emissions but also by terrestrial biospheric activities mainly in China.

1. Introduction

Measurements of atmospheric CO_2 show a long-term increasing trend, mainly due to fossil fuel combustion (Keeling et al., 1989; Keeling and Whorf, 2005). Interannual variations superimposed on the long-term trend have also been observed, associated mainly with the El Niño-Southern Oscillation (ENSO) events (Bacastow et al., 1980; Keeling and Revelle, 1985; Conway et al., 1994) and volcanic eruptions (Keeling et al., 1995; Patra et al., 2005a) that cause changes in the terrestrial biospheric and oceanic CO_2 fluxes (Nakazawa et al., 1993; Francey et al., 1995; Keeling et al., 1995, 1996; Rayner et al., 1999). CO_2 emissions from forest fires in the tropical and boreal regions have also been found to contribute to the interannual variability in the CO_2 growth rate (Langenfelds et al., 2002; Shultz, 2002; Patra et al., 2005a). It is also interesting to note that Dargaville et al. (2000), Higuchi et al. (2002), Taguchi et al. (2003) and Murayama et al. (2004) have shown that a significant portion of the year-to-year variation in atmospheric CO_2 in northern mid- to high-latitude regions can be influenced by the variation in atmospheric transport.

It has also been found that the seasonally varying CO_2 exchange between the atmosphere and the terrestrial biosphere is the main driver of the observed atmospheric seasonal CO_2 cycle, and its variation can have a significant influence on the seasonal atmospheric CO_2 concentration variability (Fung et al., 1983; Keeling et al., 1989; Nakazawa et al., 1997a). The seasonality of the CO_2 exchange between the atmosphere and the oceans, as well as that of fossil fuel combustion, is also partly responsible for the seasonal CO_2 cycle and its variation (Heimann et al., 1989).

The data from precise measurements of the atmospheric CO_2 concentration over a wide geographical area have been used to constrain the global carbon budget (Tans et al., 1989, 1990; Fan et al., 1998; Bousquet et al., 2000; Gurney et al., 2002; Patra et al., 2005b,c). However, the present measurement stations

*Corresponding author.
e-mail: zhangx@caos-a.geophys.tohoku.ac.jp
DOI: 10.1111/j.1600-0889.2007.00288.x

of atmospheric CO_2 are unevenly distributed on the globe, and only a limited number of stations exist on the continents and in the equatorial region. East Asia is a region of rapid economic development, with a consequential increase in the greenhouse gas emissions over the coming decades (Van Aardenne et al., 1999). In order to monitor the changes in the CO_2 emission in East Asia, we initiated a regular flask air sampling program onboard a ferry in the southernmost part of Japan in June 1993. We expect the data to provide an indication of changes in the natural and anthropogenic emissions of CO_2 over the Asian Continent.

In this paper, we show temporal variations of atmospheric CO_2 in the subtropical region of East Asia for the period June 1993–April 2005 and, with the aid of backward trajectory analysis and a three-dimensional atmospheric transport model, interpret them in terms of atmospheric transport and CO_2 flux regions.

2. Air sampling and CO_2 concentration analysis

Air sampling was begun in June 1993 aboard a ferry named 'Hateruma' plying between Ishigaki Island and Hateruma Island located at the southern end of the Japanese Archipelago and east of Taiwan, as shown in Fig. 1, and the sampling still continues. In this area, northerly winds prevail from October to March, while southerly winds dominate during rest of the year. The ferry 'Hateruma' usually departs from the port of Ishigaki around 10 a.m. and arrives at the port of Hateruma around noon, and two flask samples are obtained over this 2-hr period. An air intake is set on the windward wing of the bridge located at the stem, and the bridge doors are closed to prevent contamination from the ship itself. An air sample is taken from the intake and pressurized into a 350-ml stainless-steel flask to about 0.35 MPa by using an electric diaphragm pump after passing a sufficient amount of air through it. Water vapour is removed by forcing the air through magnesium perchlorate ($Mg(ClO_4)_2$). Two flask samples are collected every two weeks during one of the ferry trips from Ishigaki to Hateruma. The flask samples are returned to our laboratory for CO_2 concentration analysis. All flasks are evacuated in the laboratory at 1×10^{-3} Pa for 1 hour at 120 °C before they are shipped out for air sample collection.

Our procedures for the CO_2 concentration analysis have been described in detail elsewhere (Tanaka et al., 1983, 1987; Nakazawa et al., 1993). Therefore, only a brief description of the procedures is given here. The CO_2 concentrations of the air samples are determined against our CO_2 standard gases using a non-dispersive infrared analyser with a precision of ±0.01 ppmv within two weeks of the sampling. Our standard gases consist of primary, secondary and working, and all gases are CO_2-in-air mixtures. For the period of our study, three working standards were used, and their CO_2 concentrations ranged over 30 ppmv, so that the CO_2 concentrations of the air samples stayed between the high and low values of the working standards. The CO_2 concentrations of the working standard gases were determined using the secondary standards before and after their use, and it was confirmed that the concentration drifts were within ±0.05 ppmv. The secondary standard gases were calibrated against our primary standards prepared gravimetrically with uncertainties of ±0.1 ppmv using a precise balance and three-stage dilution.

3. Data analysis

The CO_2 concentration values of the two samples collected on the same day were simply averaged to obtain a daily value. A fitted curve composed of a long-term trend and an average seasonal cycle was derived by applying a digital filtering technique (Nakazawa et al., 1997b) to the data record, and a standard deviation of the data from the fitted curve was calculated. Any data lying outside ±3 *SD* were regarded as outliers and excluded from the record. This procedure was repeated until no outliers were identified. These outlier values were likely a result of contamination by ship and other activities that were not of background nature. A total of 45 data points were rejected as outliers by this method, corresponding to 9% of all the measurements. After the outliers were removed, the curve fitting method was applied to the remaining CO_2 values to obtain the long-term trend, the average seasonal cycle and its interannual variability.

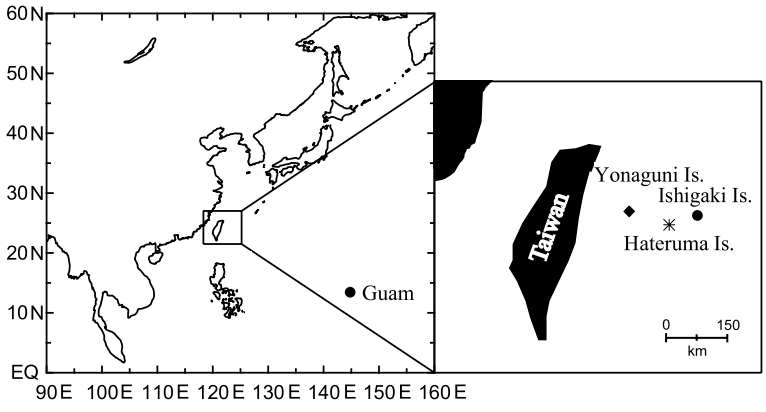

Fig. 1. Map showing our sampling location and its surroundings.

Our data were also compared to the continuous CO_2 measurements taken by the National Institute for Environmental Studies (NIES) on Hateruma Island (HTR: 123°48′E, 24°03′N) from 1993 to 2001, as well as to those obtained by the Japan Meteorological Agency (JMA) on Yonaguni Island (YGN: 123°01′E, 24°28′N)) from 1997 to 2005 (http://gaw.kishou.go.jp/). Daily mean CO_2 values from these sites were used in the comparison. However, we also compared the 11:00 a.m. and noon hourly values on those days that corresponded to the days when our samples were taken. In addition to the two sites mentioned above, we made references to the weekly flask data obtained by the National Oceanic and Atmospheric Administration/Earth System Research Laboratory/Global Monitoring Division (NOAA/ESRL/GMD) on Guam Island (GAM: 144°47′E, 13°26′N) from June 1993 to 2004 (http://gaw.kishou.go.jp/, ftp://ftp.cmdl.noaa.gov/).

Insight into the variability of a CO_2 time series requires an understanding of how it is influenced by various CO_2 sources. For this purpose, we employed a global three-dimensional atmospheric transport model with fossil fuel CO_2 emissions and terrestrial biospheric and oceanic CO_2 fluxes. The atmospheric transport model used is essentially the same as the one used in Fujita et al. (2003), except that the spatial resolution was increased from 2.5° × 2.5° to 1° × 1° in order to obtain a better identification of atmospheric CO_2 concentration variations produced by spatially localized CO_2 fluxes. Also, instead of the 1997 ECMWF meteorological data used to drive the model in the Fujita et al. study, we used the 6-hourly NCEP/NCAR reanalysis data for 1993–2004. The fossil fuel CO_2 emissions were taken from the CDIAC database (Marland et al., 2003), the oceanic CO_2 fluxes were based on Takahashi et al. (2002), and the terrestrial biospheric CO_2 fluxes were calculated using the Biome BioGeochemical Cycle model (Biome-BGC) version 4.1.2. (Thornton et al., 2002) driven offline by the NCEP/NCAR reanalysis data.

4. Results and discussion

The CO_2 concentrations measured on the ferry from June 1993 to April 2005 are plotted in Fig. 2, together with the best-fitting curve to the data and the long-term trend (Our data will be available from the World Data Centre for Greenhouse Gases: http://gaw.kishou.go.jp/). For comparison, curves fitted to the daily mean CO_2 data from HTR and YGN, as well as to the flask data from GAM, are also displayed. It is evident that the CO_2 concentration increases secularly at all sites, accompanied by the seasonal cycle and interannual variations. It is evident that, overall, the CO_2 concentration from GAM is lower than those from the ferry, HTR and YGN. Our results also show that the CO_2 concentration from the ferry is lower and higher in the spring and summer of 1998, respectively, compared with values in the corresponding seasons of other years. This feature is not visibly apparent in the CO_2 variations at GAM, and the spring-time low concentrations are clearly seenin the records from HTR and YGN but not the summertime high. The summertime high values similar to those observed on the ferry are found only in the time series of selected hourly mean CO_2 concentrations at HTR and YGN (not shown). The latter result indicates that the high CO_2 concentrations observed on the ferry in the summer of 1998 could be attributable to our temporally sparse air sampling. Observational results and their discussion are given below in more detail, especially in terms of the annual mean value, the long-term trend and the seasonal cycle of the CO_2 concentration.

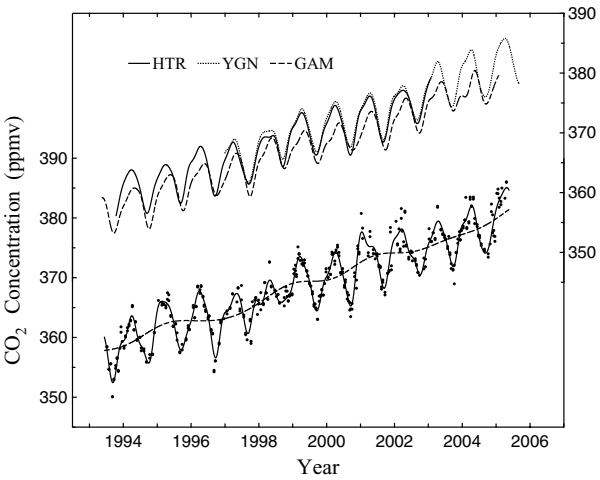

Fig. 2. CO_2 concentrations measured on the ferry (solid circle), the best-fitting curve to the data (solid line) and the long-term trend (dashed line). Curves fitted to the CO_2 concentrations measured on Hateruma Island (HTR), Yonaguni Island (YGN) and Guam Island (GAM) are also shown in the upper part of the figure.

4.1. *Annual mean value and long-term trend of CO_2 concentration*

The annual mean CO_2 concentrations and the average growth rates derived from the best-fitting curves of all the above-mentioned data records are summarized in Table 1. Our annual mean CO_2 concentrations are in close agreement with the values from the two data records for HTR, as well as from the selected hourly mean CO_2 concentration data for YGN. At YGN, the annual mean CO_2 values calculated from the daily mean concentration data are higher by about 1 ppmv than those from the selected hourly mean data, except for 2000 and 2001 when the values for the two datasets are almost the same, probably due to the influence of the diurnal cycle. It is also apparent that the annual means are lower by about 1.4 ppmv at GAM compared to the other three locations, reflecting different air mass influence over different regions; for example, air masses in the southernmost part of Japan are transported from the Eurasian Continent with anthropogenic and natural CO_2 in the winter and from the

Table 1. Annual mean CO_2 concentrations (ppmv) and mean CO_2 growth rates (ppmv yr^{-1}) calculated from the best-fitting curves of the data taken on the ferry (This study), Hateruma Island (HTR), Yonaguni Island (YGN) and Guam Island (GAM)

Years	This study	HTR	HTR[a]	YGN	YGN[b]	GAM
1994	360.1	360.7	360.5	–	–	358.3
1995	362.6	362.4	362.3	–	–	360.3
1996	362.8	364.3	364.0	–	–	362.4
1997	364.5	365.1	364.6	365.8	364.5	363.5
1998	367.6	368.1	368.0	368.8	367.9	366.5
1999	369.4	370.3	370.3	370.8	369.8	367.8
2000	370.7	371.2	371.0	371.8	371.8	369.2
2001	373.5	373.0	372.8	373.3	373.5	370.9
2002	374.5	375.2	374.9	375.6	374.5	373.1
2003	376.2	–	–	378.4	377.5	375.9
2004	378.4	–	–	380.1	378.3	377.4
Mean growth rate	1.8	1.8	1.8	2.0	1.9	1.9

[a]The results obtained from selected hourly mean CO_2 concentration data.

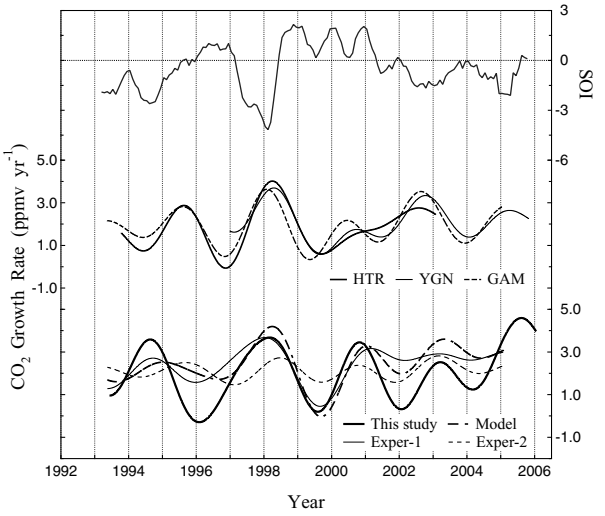

Fig. 3. Growth rates of the CO_2 concentration observed on the ferry (This study), Hateruma Island (HTR), Yonaguni Island (YGN) and Guam Island (GAM), and 5-month running mean of the monthly Southern Oscillation Index values (SOI). The CO_2 growth rate simulated by the three-dimensional atmospheric transport model is also shown (Model), together with the results of two model experiments; 1997 wind field, interannually varying seasonal biospheric flux (Exper-1) and interannually varying wind field, annually invariant seasonal biospheric flux (Exper-2).

Pacific Ocean in the summer, while easterly winds with low CO_2 concentrations usually prevail over Guam Island throughout the year.

As seen from Table 1, our results show that the CO_2 concentration increases from 360.1 ppmv in 1994 to 378.4 ppmv in 2004. The average growth rate of the CO_2 concentration is calculated to be 1.8 ppmv yr^{-1}, which is very close to that at GAM for the same period. More detailed inspection of the table indicates that the CO_2 growth rate varies interannually at all locations.

The growth rate of the CO_2 concentration measured in this study is shown in Fig. 3, together with those at HTR, YGN and GAM. Also shown are the growth rate calculated by using the three-dimensional atmospheric transport model for our sampling location, and a 5-month running mean of the monthly Southern Oscillation Index (SOI) values (http://www.cpc.ncep.noaa.gov/data/indics/soi). The CO_2 growth rate observed on the ferry reaches high values in 1994, 1997/1998, 2002/2003 and 2004/2005 in association with ENSO events. High growth rates are also found in 2000/2001 when no ENSO event occurred. This temporal behaviour of the growth rate is similar to those at HTR, YGN and GAM, except that there is a difference of about 1 yr between the occurrence of a maximum in 1994 on the ferry and that in 1995 at the other sites. The difference in the timing of the growth rate maximum may be due to our low frequency air sampling.

The CO_2 concentrations calculated using the atmospheric transport model show an average growth rate of about 2.2 ppmv yr^{-1} for the study period, which is larger than our observed value by 0.4 ppmv yr^{-1}. The difference between the calculated and the observed average growth rates is quantitatively attributable to insufficient uptake of atmospheric CO_2 by the oceans and/or by the terrestrial biosphere in the model. The model calculation also shows that the CO_2 growth rate varies interannually, with high values in 1997/1998, 2000/2001 and 2002/2003 and low values in 1999 and 2001/2002. Slightly high and low growth rates are also found in 1994/1995 and 1996/1997, respectively. This temporal behaviour is in a general agreement with the observational results.

In our model calculation, the same monthly oceanic CO_2 flux data set was repeatedly used, while the terrestrial biospheric CO_2 flux and the wind field varied from year-to-year. Interannual variation in the fossil fuel CO_2 emission is known to be small (Marland et al., 2003). Within the context of the model design, the interannual variation superimposed on the long-term CO_2 increase trend can be attributed to the interannual variations in atmospheric transport and terrestrial biospheric CO_2 flux, mainly in association with ENSO events (Nakazawa et al., 1993; Keeling et al., 1995, 1996a,b; Dargaville et al., 2000; Higuchi et al., 2002; Taguchi et al., 2003; Murayama et al., 2004). In order to examine the relative contributions of these effects, we performed two numerical experiments with the model, for which the terrestrial biospheric CO_2 flux and the wind field were assumed to be interannually variable and invariable, respectively (Exper-1), and vice versa (Exper-2); the Biome-BGC CO_2 flux data averaged over the 1990s were used for the interannually invariable terrestrial biospheric fluxes, and the 1997 wind data were employed to give the interannually invariable transport field. The results are displayed in Fig. 3. The results of Exper-1 (1997 wind

field, interannually varying seasonal biospheric flux) show interannual variation of the CO_2 growth rate larger than that obtained in Exper-2 (interannually varying wind field, annually invariant seasonal biospheric flux) before 2001, while the situation is reversed after 2001. The CO_2 growth rates from Exper-1 and Exper-2 are generally in phase after around 1997, giving an additive effect closer to the observed growth rate variation. However, prior to 1997, the model growth rates are out of phase resulting in a relatively constant growth rate, unlike the observed growth rates on the ferry and at HTR and GAM shown in Fig. 3.

The differences, both in magnitude and phase, between the observed and simulated growth rates can be caused by many factors. One possible cause for the differences can be due to the fact that, in the model experiments, we did not provide interannually varying oceanic CO_2 flux. For example, Feely et al. (1999) from their pCO_2 measurements, and Bousquet et al. (2000) and Patra et al. (2005c) from their inverse model analyses, found that there is a significant interannual variation in the oceanic CO_2 flux. Wong et al. (1993) and Rayner et al. (1999) pointed out that the oceanic CO_2 flux in the tropical Pacific is significantly influenced by ENSO events; this could have a large impact on the CO_2 concentration in our observational area since it is influenced by air masses from the tropical Pacific from late spring to early autumn.

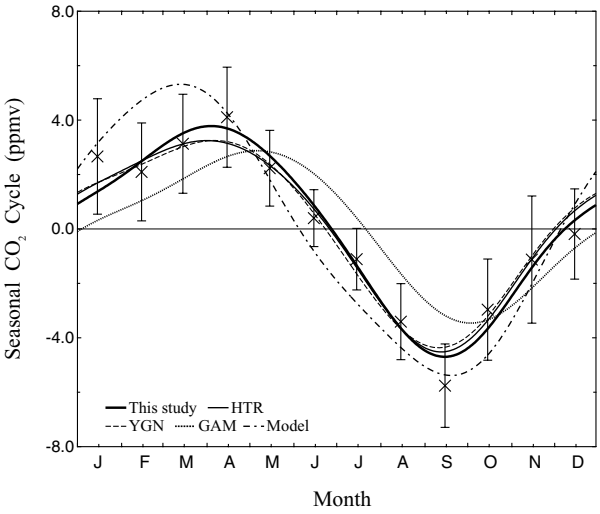

Fig. 4. Average seasonal cycles of the CO_2 concentration observed on the ferry (This study), Hateruma Island (HTR), Yonaguni Island (YGN) and Guam Island (GAM). The seasonal CO_2 cycle calculated by the three-dimensional atmospheric transport model for our sampling location is also shown (Model). Detrended monthly mean CO_2 concentrations and their standard deviations obtained on the ferry are represented by crosses and vertical bars, respectively.

4.2. Seasonal CO_2 cycle

The average seasonal cycle of the CO_2 concentration observed on the ferry is shown in Fig. 4, together with those at HTR, YGN and GAM. The results presented for HTR and YGN were derived using daily mean CO_2 data. More information on the seasonal CO_2 cycle is summarized in Table 2. The seasonal amplitude is found to be 8.5 ppmv on the ferry, which is in agreement with 7.8 and 7.6 ppmv derived, respectively, from the daily mean CO_2 data at HTR and YGN. The slight differences in the amplitude between the two sites and the ferry are likely due to the low frequency sampling of the ferry data. Indeed, as shown in Table 2, the seasonal amplitudes calculated from the selected hourly data at HTR and YGN are larger than those obtained from the daily mean values. As a further analysis, we calculated monthly standard deviations of the detrended data for HTR, and found that the standard deviations for spring (March–May) and autumn (October and November) are clearly larger than those for the remaining seasons, probably due to seasonal alternation of prevailing air masses. This supports our conjecture and that the infrequent air sampling in the two seasons is responsible for the above-mentioned larger seasonal amplitude obtained on the ferry.

The average seasonal CO_2 cycle observed on the ferry reaches the maximum in early April and the minimum in mid-September. The drawdown and buildup zero-crossing dates of the seasonal cycle occur in late June and early December, respectively, with a time span of 164 d. These seasonal features are similar to those at HTR and YGN, except for the selected hourly data at YGN which show the seasonal cycle with an earlier phase.

Compared with our results from the ferry, the seasonal CO_2 cycle at GAM is clearly different; the amplitude is 6.3 ppmv which is smaller by about 2 ppmv, and the phase is delayed by approximately 1 month. The difference between the seasonal cycles at the two locations is mainly attributable to the fact that air masses arriving at the respective locations are different. As mentioned above, our sampling location is usually influenced by continental air masses except for summer when air masses come from low latitudes in the Pacific, while air masses traversing over the equatorial Pacific always prevail at GAM.

The average seasonal CO_2 cycle calculated using the atmospheric transport model for our sampling location is also shown in Fig. 4 (also see Table 2). The calculated seasonal cycle shows the maximum and minimum concentrations in mid-March and mid-September, respectively, with a peak-to-peak amplitude of 10.7 ppmv. Its drawdown and buildup zero-crossings occur in early June and early December, respectively, with a time span of 184 d. Compared with the observed seasonal cycle, the calculated seasonal amplitude is larger by about 2 ppmv, and the maximum concentration appears earlier by about half a month, while the minimum concentration occurs around the same time. The time interval between the zero-crossings is longer than observed by 20 d. The overall difference between the observed and the calculated average seasonal CO_2 cycles is due mainly to the seasonality of the terrestrial biospheric CO_2 flux given by the

Table 2. Information on the seasonal CO_2 cycles observed on the ferry (This study), Hateruma Island (HTR), Yonaguni Island (YGN) and Guam Island (GAM) and calculated by the three-dimensional atmospheric transport model for our sampling location (Model)

	This study	HTR	HTR[a]	YGN	YGN[a]	GAM	Model
Amplitude (ppmv)	8.5	7.8	8.5	7.6	8.5	6.3	10.7
Maximum concentration	4 April	1 April	7 April	6 April	20 March	6 May	14 March
Minimum concentration	15 September	12 September	12 September	11 September	8 September	13 October	19 September
Zero-crossing (drawdown)	28 June	26 June	29 June	23 June	9 June	22 July	5 June
Zero-crossing (buildup)	9 December	2 December	5 December	1 December	19 November	4 January	6 December
Time interval between zero-crossings (d)	164	159	159	161	163	165	184

[a]The results obtained from selected hourly mean CO_2 concentration data.

Biome-BGC model, and the interannually variable wind field has a minor effect on the average seasonal CO_2 cycle.

4.3. Low CO_2 concentrations in spring of 1998

As mentioned earlier in the paper, the CO_2 concentration measured on the ferry shows relatively lower spring values in 1998 compared to other years. As can be seen in Fig. 2, the springtime low CO_2 concentrations are also observed at HTR and YGN. To elucidate the cause of this anomalous CO_2 concentration event, we performed a series of 5-d back trajectory calculations using a three-dimensional isentropic backward trajectory model (Maksyutov and Inoue, 2000) for the spring of 1997, 1998, 1999 and 2000. In this analysis, the model was driven by the 12-hr NCEP reanalysis data with a horizontal resolution of 2.5° × 2.5°. Air parcels were released from approximately 500 m height at noon (LT) each day from March to May, and the number of air parcels passing through each horizontal grid (1° × 1°) were counted. By examining the horizontal distribution of air parcels counted, we find the air arriving at the ferry came mainly from southeast during the spring of 1998 (Fig. 5), unlike other years (1997, 1999 and 2000) when westerly and northwesterly transport from the Asian continent was dominant (not shown). This suggests the importance of transport in accounting for some part of the interannual variation in the CO_2 concentration observed at monitoring stations (Taguchi et al., 2003).

Zhang et al. (1997) showed that the frequency of cold surges across China is minimal during and right after ENSO events. Liu et al. (2003) also found that the number of cold surges across China was reduced in March 1998. Their findings suggest that the air transport from the Asian Continent was weaker in the spring of 1998 in association with the 1997/1998 ENSO event, allowing maritime air masses with relatively low CO_2 concentrations to prevail over the region sampled by the ferry.

4.4. Interpretation of very high and low CO_2 concentration events

A visual inspection of the CO_2 concentration record obtained on the ferry indicates relatively high and low values. It is of interest therefore to find causes of such extreme values. The following data are selected for investigation since they are found to lie outside the $\pm 2\sigma$ fitted curve obtained by the digital filtering technique mentioned earlier in the paper: six data (December 7, 1993, February 24, 1999, December 2, 2000, January 23, 2001, January 17, 2002 and March 16, 2002) and 3 data (September 4, 1993, September 3, 1996 and September 16, 2000) are accordingly defined as exceptionally high and low CO_2 concentration events, respectively. This selection result indicates that high CO_2 concentration events occur mainly in the winter season, while low CO_2 concentration events are found in September.

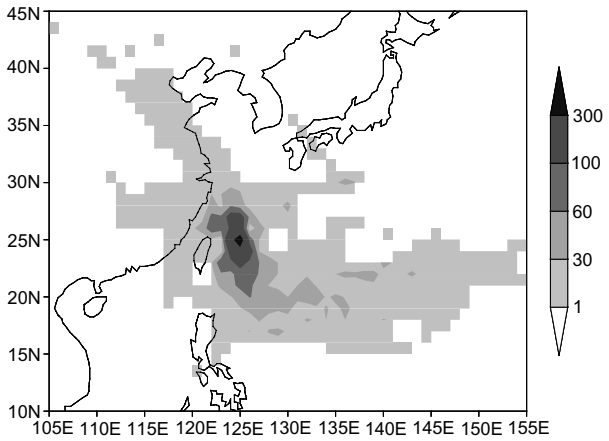

Fig. 5. Number of air parcels passing through each horizontal grid (1° × 1°), obtained from 5-d backward trajectory calculations for the air parcels released from 500 m over our sampling location at noon each day from March to May 1998.

Figure 6 shows 5-d backward trajectories for the events selected above. Figure 7 depicts the surface CO_2 concentration distributions in Asia calculated by the three-dimensional atmospheric transport model for December 7, 1993, January 23, 2001, March 16, 2002 and September 16, 2000, as well as those averaged over 5 d prior to the above dates. It is evident from Figs. 6 and 7 that the high-CO_2 event of December 7, 1993 observed on the ferry is caused by a transport of air with high CO_2 concentrations from mid-eastern China, a fossil fuel CO_2

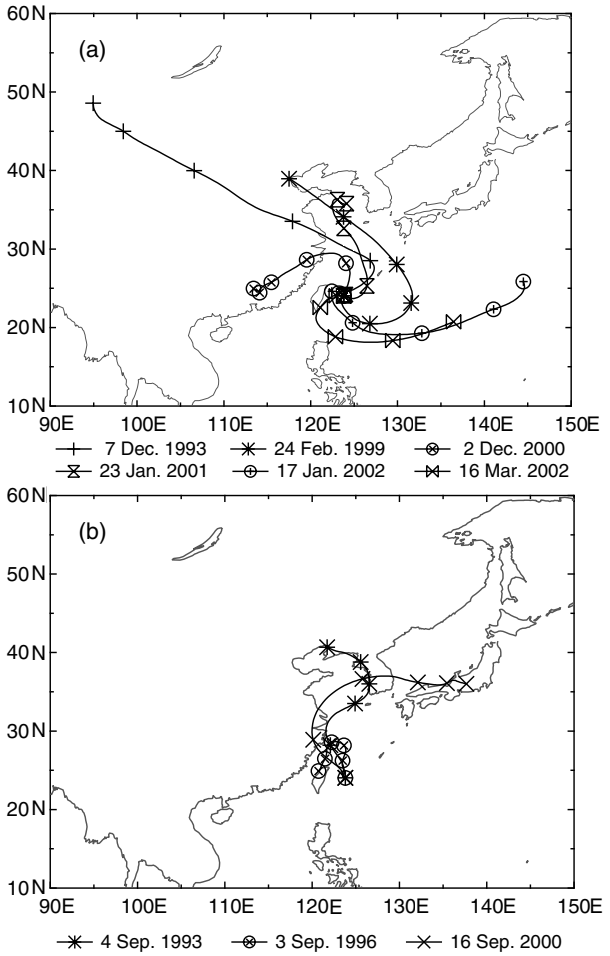

Fig. 6. Five-day backward trajectories of air parcels released from our sampling location at noon of the respective dates.

emission region. A transport of CO_2-rich air mass from Europe through Siberia could have also contributed to the December 7 event.

As for January 23, 2001, the trajectory analysis suggests that air mass originating in the Yellow Sea reaches our sampling location after passing over the East China Sea. As seen in Fig. 7, the CO_2 concentration is considerably high in those areas due to transport of fossil fuel and terrestrial biospheric CO_2 from mid-eastern China. A similar situation is found for the case of February 24, 1999, but in this case the influence of terrestrial biospheric CO_2 is found to be more pronounced than in January, based on the model calculation results. On the other hand, air masses arrived at our sampling location on January 17, 2002 and March 16, 2002 are transported mostly over the Pacific Ocean for 5 d, so that the opportunity of being influenced by a high CO_2 source seems to be limited. However, a detailed inspection of the trajectories indicates that the air masses arriving at our sampling location passed through the vicinity of Taiwan where the CO_2 concentration is considerably high, as seen in Fig. 7. Therefore, these two cases reflect influences of outflow of terrestrial biospheric and fossil fuel CO_2 from China and Southeast Asia, as well as by CO_2 emissions in Taiwan itself.

To interpret the relatively low CO_2 concentration events found in September, we employ the same strategy as above. As seen in Fig. 6, the results show that air comes from northern China through the Korean Peninsula and the East China Sea on September 4, 1993, circularly from Taiwan on September 3, 1996 and from the central part of Japan through the Korean Peninsula and the east side of central China on September 16, 2000. These trajectories are found to pass through areas of low CO_2 concentration, as calculated by the transport model. The CO_2 concentration field calculated for September 16 is shown in Fig. 7 as an example. Such low CO_2 concentrations are thought to be produced by photosynthetic activities of the terrestrial biosphere in the Eurasian Continent and the surrounding regions.

5. Conclusions

To examine temporal variations of atmospheric CO_2 in the subtropical region of East Asia, as well as the influence of anthropogenic and natural CO_2 emissions in the Eurasian Continent, we collected air samples almost biweekly on board a ferry plying between Ishigaki Island and Hateruma Island in the southernmost part of Japan from June 1993 to April 2005. The CO_2 concentration data obtained were analysed in terms of the long-term trend, its interannual variability and the seasonal cycle, and the results were compared with those from continuous measurements on Hateruma Island and Yonaguni Island, as well as from flask sampling on Guam Island. We also interpreted the observed variations of the CO_2 concentration using a backward trajectory analysis and a global three-dimensional atmospheric transport model. The results obtained in this study are summarized as follows:

1. The annual mean CO_2 concentration increases from 360.1 ppmv in 1994 to 378.4 ppmv in 2004, with an average growth rate of 1.8 ppmv yr^{-1}. This growth rate is in good agreement with those observed at the Hateruma, Yonaguni and Guam sites. The average seasonal cycle shows the maximum concentration in early April and the minimum concentration in mid-September, with a peak-to-peak amplitude of 8.5 ppmv. The observed seasonal CO_2 cycle agrees fairly well with those at Hateruma and Yonaguni, but with respect to Guam the seasonal amplitude is larger by about 2 ppmv and the phase is earlier by 1 month.

2. The measured CO_2 concentration shows significantly lower values in the spring of 1998, as compared with those of contiguous years. It is suggested that this concentration anomaly is related to changes in atmospheric circulation induced by the strong 1997/1998 ENSO event, by which the transport of polluted air from the Asian Continent is much reduced, in

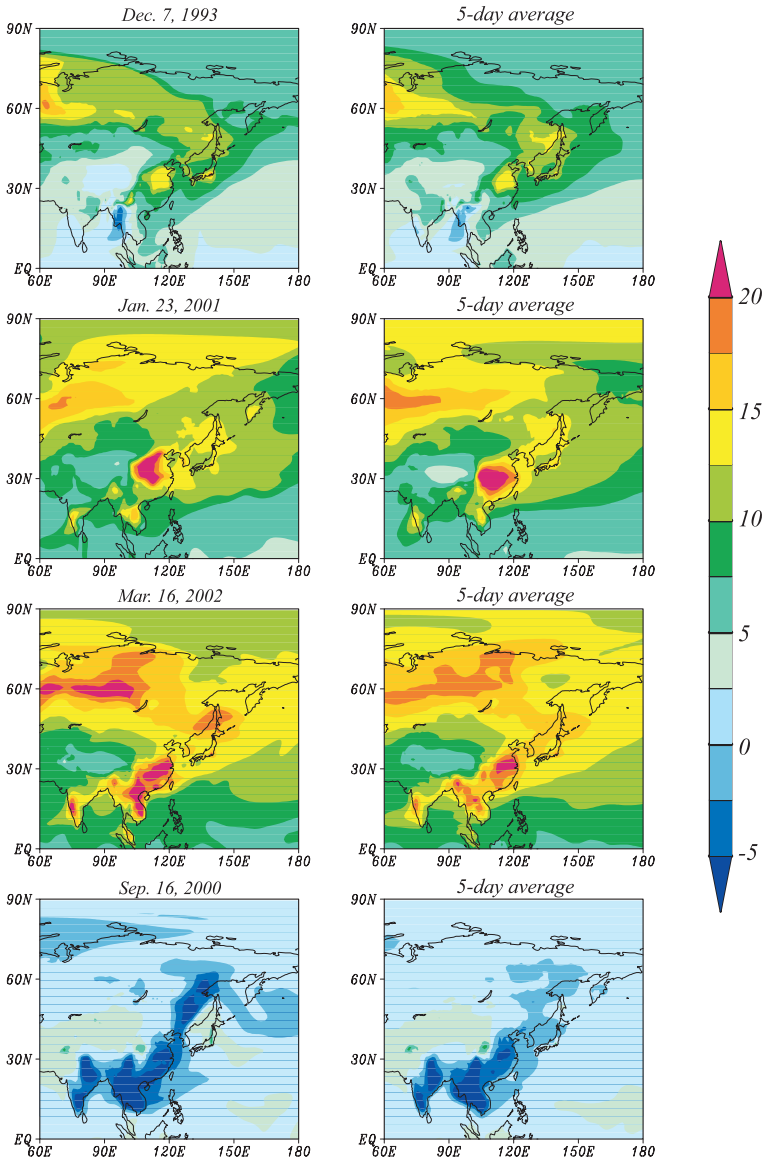

Fig. 7. CO_2 concentration distributions calculated by the three-dimensional atmospheric transport model for December 7, 1993, January 23, 2001, March 16, 2002 and September 16, 2000, and those averaged for 5 d before the respective dates. The CO_2 concentrations are represented as deviations from the South Pole values.

comparison with the transport of western Pacific air masses with low CO_2 concentrations.

3. Very high and low CO_2 concentrations are sometimes observed in winter and early spring (December to March) and in September, respectively. The backward trajectory analysis and the CO_2 concentration distributions calculated using the three-dimensional atmospheric transport model suggest that the high CO_2 concentrations occur due to transport of air masses affected by anthropogenic activities and terrestrial biospheric respiration in China, while the low CO_2 concentrations occur due to transport of air masses influenced by terrestrial biospheric photosynthesis mainly in China and Southeast Asia.

4. A clear seasonal CO_2 cycle is calculated for our sampling location by the atmospheric transport model. Compared with the observed seasonal CO_2 cycle, the simulated maximum concentration appears earlier by 1 month, while the minimum concentration is found at a similar time of the year as the observation, and the model amplitude is larger by about 2 ppmv. The calculated and observed growth rates of the CO_2 concentration show a similar temporal behaviour, but apparent differences are also found, presumably due to year-by-year changes in the oceanic CO_2 flux not included in the model.

East Asia is one of the most economically rapidly developing regions in the world. Human activities in this region would significantly affect future levels of the atmospheric CO_2 concentration. Therefore, it is of special importance to evaluate anthropogenic CO_2 emissions from this region, as well as to continue to monitor the atmospheric CO_2 concentration precisely for its validation.

6. Acknowledgments

We express our sincere thanks to the staffs of Hateruma-kaiun & Co. for their cooperation in collecting air samples for a long time. This study was partly supported by the Ministry of Education, Science, Sports and Culture, Grants-in-Aid for Creative Scientific Research, 2005, 17GS0203 and the Research Institute for Humanity and Nature Research Project 2-1.

References

Bacastow, R. B., Adams, J. A., Keeling, C. D., Moss, D. J., Whorf, T. P. and co-authors. 1980. Atmospheric carbon-dioxide, the Southern Oscillation, and the weak 1975 El-Nino. *Science* **210**, 66–68.

Bousquet, P., Peylin, P., Ciais, P., Quere, C. L., Freidlingstein, P. and co-authors. 2000. Regional changes in carbon dioxide fluxes of land and oceans since 1980. *Science* **290**, 1342–1346.

Conway, T. J., Tans, P. P., Waterman, L. S., Thoning, K. W., Kitzis, D. R. and co-authors. 1994. Evidence for interannual variability of the carbon cycle from the NOAA/CMDL global air sampling network. *J. Geophys. Res.* **99**, 22,831–22,855.

Dargaville, R., Law, R. M. and Pribac, F. 2000. Implications of interannual variability in atmospheric circulation on modeled CO_2 concentrations and source estimates. *Global Biogeochem. Cycles* **14**, 931–943.

Fan, S., Gloor, M., Mahlman, J., Pacala, S., Sarmiento, J. and co-authors. 1998. A large terrestrial carbon sink in North America implied by atmospheric and oceanic CO_2 data and models. *Science* **282**, 442–446.

Feely, R. A., Wanninkhof, R., Takahashi, T. and Tans, P. P. 1999. Influence of El Nino on the equatorial Pacific contribution to atmospheric CO_2 accumulation. *Nature* **398**, 597–601.

Francey, R. J., Tans, P. P., Allison, C. E., Enting, I. G., White, J. W. C. and co-authors. 1995. Changes in oceanic and terrestrial carbon uptake since 1982. *Nature* **373**, 326–330.

Fujita, D., Ishizawa, M., Maksyutov, S., Thornton, P. E., Saeki, T. and co-authors. 2003. Inter-annual variability of the atmospheric carbon dioxide concentrations as simulated with global terrestrial biosphere models and an atmospheric transport model. *Tellus* **55B**, 530–546.

Fung, I., Prentice, K., Matthews, E., Lerner, J. and Russell, G. 1983. Three-dimensional tracer model study of atmospheric CO_2: response to seasonal exchanges with the terrestrial biosphere. *J. Geophys. Res.* **88**, 1281–1294.

Gurney, K. R., Law, R. M., Denning, A. S., Rayner, P. J., Baker, D. and co-authors. 2002. Towards robust regional estimates of CO_2 sources and sinks using atmospheric transport models. *Nature* **415**, 626–630.

Heimann, M., Keeling, C. D. and Tucker, C. J. 1989. A three-dimensional model of atmospheric CO_2 transport based on observed winds: **3**. Seasonal cycle and synoptic time scale variations. In: *Aspects of Climate Variability in the Pacific and the Western Americans Geophys. Monogr*. **55** (ed. Peterson, D. H.). Am. Geophys. Union, Washington DC, 277–303.

Higuchi, K., Murayama, S. and Taguchi, S. 2002. Quasi-decadal variation of the atmospheric CO_2 seasonal cycle due to atmospheric circulation changes: 1979–1998. *Geophys. Res. Lett.* **29**, doi:10.1029, 2001GL013751.

Keeling, C. D. and Revelle, R. 1985. Effects of El-Niño Southern Oscillation on the atmospheric content of carbon dioxide. *Meteoritics* **20**, 437–450.

Keeling, C. D. and Whorf, T. P. 2005. Atmospheric CO_2 records from sites in the SIO air sampling network. In *Trends: A Compendium of Data on Global Change*. Carbon Dioxide Information Analysis Center, Oak Ridge National Laboratory, U.S. Department of Energy, Oak Ridge, Tenn., U.S.A.

Keeling, C. D., Bacastow, T. R., Carter, A. F., Piper, S. C., Whorf, T. P. and co-authors 1989. A three-dimensional model of atmospheric CO_2 transport based on observed winds: 1. Analysis of observational data. In: *Aspects of Climate Variability in the Pacific and the Western Americas Geophys. Monogr.* **55** (ed. Peterson, D. H.). Am. Geophys. Union, Washington DC, 165–236.

Keeling, C. D., Whorf, T. P., Wahlen, M. and Van der Pflicht, J. 1995. Interannual extremes in the rate of rise of atmospheric carbon dioxide since 1980. *Nature* **375**, 666–670.

Keeling, C. D., Chin, J. F. S. and Whorf, T. P. 1996. Increased activity of northern vegetation inferred from atmospheric CO_2 measurements. *Nature* **382**, 146–149.

Langenfelds, R. L., Francey, R. J., Pak, B. C., Steele, L. P., Lloyd, J. and co-authors. 2002. Interannual growth rate variations of atmospheric CO_2 and its $\delta^{13}C$, H_2, CH_4, and CO between 1992 and 1999 linked to biomass burning. *Global Biogeochem. Cycles* **16**(3), 1048, doi:10.1029/2001GB0011466.

Liu, H., Jacob, D. J., Bey, I., Yantosca, R. M. and Duncan, B. N. 2003. Transport pathways for Asian pollution outflow over the Pacific: interannual and seasonal variations. *J. Geophys. Res.* **108**, 8786, doi:10.1029/2002JD003102.

Maksyutov, S. and Inoue, G. 2000. Vertical profiles of radon and CO_2 simulated by the global atmospheric transport model. In: *CGER Supercomputer activity report, CGER-I039–2000, CGER NIES* Volume 7. Tsukuba, Japan, 39–41.

Marland, G.., Boden, T. A. and Andres, R. J. 2003. Global, regional, and national CO_2 emissions. In: *Trends: A Compendium of Data on Global Change.* Carbon Dioxide Information Analysis Center, Oak Ridge National Laboratory, U.S. Department of Energy, Oak Ridge, Tenn., U.S.A.

Murayama, S., Taguchi, S. and Higuchi, K. 2004. Interannual variation in the atmospheric CO_2 growth rate: Role of atmospheric transport in the Northern Hemisphere. *J. Geophys. Res.* **109**, D02305.

Nakazawa, T., Morimoto, S., Aoki, S. and Tanaka, M. 1993. Time and space variations of the carbon isotopic ratio of tropospheic carbon dioxide over Japan. *Tellus* **45B**, 258–274.

Nakazawa, T., Morimoto, T., Aoki, S. and Tanaka, M. 1997a. Temporal and spatial variations of the carbon isotopic ratio of atmospheric carbon dioxide in the Western Pacific region. *J. Geophys. Res.* **102**, 1271–1285.

Nakazawa, T., Ishizawa, M., Higuchi, K. and Trivett, B. A. N. 1997b. Two curve fitting methods applied to CO_2 flask data. *Environmetrics* **8**, 197–218.

Patra, P. K., Maksyutov, S. and Nakazawa, T. 2005a. Analysis of atmospheric CO_2 growth rates at Mauna Loa using inverse model derived CO_2 fluxes. *Tellus* **57B**, 357–365.

Patra, P. K., Maksyutov, S., Ishizawa, M., Nakazawa, T. and Inoue, G. 2005b. Effects of biomass burning and meteorological

conditions on land-atmosphere CO_2 flux from atmospheric CO_2 inverse modeling. *Global Biogeochem. Cycle* **19**, GB3005, doi:10.1029/2004GB002258.

Patra, P. K., Maksyutov, S., Ishizawa, M., Nakazawa, Takahashi, T. and Ukita, J. 2005c. Interannual and decadal changes in the sea-air CO_2 flux from atmospheric CO_2 inverse modeling. *Global Biogeochem. Cycle* **19**, GB4013, doi:10.1029/2004GB002257.

Rayner, P. J. and Law, R. M. and Dargaville, R. 1999. The relationship between tropical CO_2 fluxes and the El Niño-Southern Oscillation. *Geophys. Res. Lett.* **26**, 493–496.

Schultz, M. G. 2002. On the use of ATSR fire count data to estimate the seasonal and interannual variability of vegetation fire emissions. *Atmos. Chem. Phys.* **2**, 387–395.

Taguchi, S., Murayama, S. and Higuchi, K. 2003. Sensitivity of interannual variation of CO_2 seasonal cycle at Mauna Loa to atmospheric transport. *Tellus* **55B**, 547–554.

Takahashi, T., Sutherland, S. C., Sweeney, C., Poisson, A., Metzl, N. and co-authors. 2002. Global sea-air CO_2 flux based on climatological surface ocean pCO_2, and seasonal biological and temperature effects. *Deep Sea Res. II* **49**, 1601–1622.

Tanaka, M., Nakazawa, T. and Aoki, S. 1983. High quality measurements of the concentration of atmospheric carbon dioxide. *J. Meteorol. Soc. Japan* **61**, 678–875.

Tanaka, M., Nakazawa, T. and Aoki, S. 1987. Time and space variations of tropospheric carbon dioxide over Japan. *Tellus* **39B**, 72–79.

Tans, P. P., Conway, T. J. and Nakazawa, T. 1989. Latitudinal distribution of the sources and sinks of atmospheric carbon dioxide derived from surface observations and an atmospheric transport model. *J. Geophys. Res.* **94**, 5151–5172.

Tans, P. P., Fung, I. Y. and Takahashi, T. 1990. Observational constraints on the global atmospheric CO_2 budget. *Science* **247**, 1431–1438.

Thornton, P. E., Law, B. E., Gholz, H. L., Clark, K. L., Falge, E. and co-authors. 2002. Modeling and measuring the effects of disturbance history and climate on carbon and water budgets in evergreen needleleaf forests. *Agric. For. Meteorol.* **133**, 185–222.

Van Aardenne, J. A., G. R., Carmichael, G. R., Levy II, H., Streets, D. and Hordijk, L. 1999. Anthropogenic NO_x emissions in Asia in the period 1990–2020. *Atmos. Environ*. **33**, 633–646.

Wong, C. S., Chan, Y.-H., Page, J. S., Smith, G. E. and Bellegay, R. D. 1993. Changes in equatorial CO_2 flux and new production estimated from CO_2 and nutrient levels in Pacific surface waters during the 1986/87 El Nino. *Tellus* **45B**, 64–79.

Zhang, Y., Sperber, K. R. and Boyle, J. S. 1997. Climatology and interannual variation of the East Asian winter monsoon: results from the 1979–95 NCEP/NCAR reanalysis. *Mon. Weather Rev.* **125**, 2605–2619.